

1 Non-climatic signal in ice core records: Lessons from Antarctic mega-dunes

2 Alexey Ekaykin^{1,2}, Lutz Eberlein³, Vladimir Lipenkov¹, Sergey Popov⁴, Mirko Scheinert³, Ludwig Schröder³,
3 Alexey Turkeev¹

4 1 – Climate and Environmental Research Laboratory, Arctic and Antarctic Research Institute, 38 Beringa
5 st., 199397, St. Petersburg, Russia

6 2 – St. Petersburg State University, 33-35, 10th line VO, 199178 St. Petersburg, Russia

7 3 – Technische Universität Dresden, Institut für Planetare Geodäsie, 01062 Dresden, Germany

8 4 – Polar Marine Geological Research Expedition, 24 Pobedy st., 198412 Lomonosov, Russia.

9 *Corresponding author:* ekaykin@aari.ru

10

11 **Abstract**

12 We present the results of glaciological investigations in the mega-dune area located 30 km to the east
13 from Vostok Station (central East Antarctica) implemented during the 58th, 59th and 60th Russian
14 Antarctic Expedition (January 2013 - January 2015). Snow accumulation rate and isotope content (δD ,
15 $\delta^{18}O$ and $\delta^{17}O$) were measured along the 2-km profile across the mega-dune ridge accompanied by
16 precise GPS altitude measurements and GPR survey. It is shown that the spatial variability of snow
17 accumulation and isotope content covaries with the surface slope. The accumulation rate regularly
18 changes by one order of magnitude within the distance < 1 km, with the reduced accumulation at the
19 leeward slope of the dune and increased accumulation in the hollow between the dunes. At the same
20 time, the accumulation rate averaged over the length of a dune wave (22 mm w.e.) corresponds well
21 with the value obtained at Vostok Station, which suggests no additional wind-driven snow sublimation
22 in the mega-dunes compared to the surrounding plateau. The snow isotopic composition is in negative
23 correlation with the snow accumulation. Analyzing $dxs/\delta D$ and $^{17}O\text{-excess}/\delta D$ slopes (where $dxs = \delta D -$
24 $8 * \delta^{18}O$ and $^{17}O\text{-excess} = \ln(\delta^{17}O/1000+1) - 0.528 * \ln(\delta^{18}O/1000+1)$), we conclude that the spatial
25 variability of the snow isotopic composition in the mega-dune area could be explained by post-
26 depositional snow modifications. Using the GPR data, we estimated the apparent dune drift velocity (4.6
27 ± 1.1 m yr⁻¹). The full cycle of the dune drift is thus about 410 years. Since the spatial anomalies of snow
28 accumulation and isotopic composition are supposed to drift with the dune, a core drilled in the mega-
29 dune area would exhibit the non-climatic 410-yr cycle of these two parameters. We simulated a vertical
30 profile of snow isotopic composition with such a non-climatic variability, using the data on the dune size
31 and velocity. This artificial profile is then compared with the real vertical profile of snow isotopic
32 composition obtained from a core drilled in the mega-dune area. We note that the two profiles are very
33 similar. The obtained results are discussed in terms of interpretation of data obtained from ice cores
34 drilled beyond the mega-dune areas.

35

36

37 **1 Introduction**

38 Large snow and ice dunes are one of the most intriguing and spectacular phenomena in Antarctica. The
39 first reports on the existence of the huge waves on the surface of the Antarctic ice sheet was made soon
40 after the beginning of the extensive exploration of the Antarctic interior during the IGY (Dolgushin,
41 1958).

42 Since then such surface undulations have been observed in different parts of the Antarctic continent – in
43 Adelie Land (Pettre et al., 1986), Dronning Maud Land (Anschutz et al., 2006;Eisen et al., 2005), Enderby
44 Land (Fujita et al., 2002), Marie Byrd Land (Whillans, 1975;Gow and Rowland, 1965), Victoria Land
45 (Frezzotti et al., 2002b;Frezzotti et al., 2002a), Queen Mary Coast (Vladimirova and Ekaykin,
46 2014;Dolgushin, 1958), Wilkes Land (Black and Budd, 1964;Goodwin, 1990) – or, simply speaking, almost
47 everywhere.

48 In 1988 Swithinbank suggested term “mega-dunes” (Swithinbank, 1988) based on their similarity to the
49 desert sand mega-dunes. At present this term is conventionally used to describe the specific dunes
50 observed in central East Antarctica (Albert et al., 2004;Alberti and Biscaro, 2010;Fahnestock et al.,
51 2000;Frezzotti et al., 2002b), which form the system of parallel ridges with the wavelength of 2-5 km,
52 the amplitude 2-8 m, and the length of the ridges of up to 100 km. One should distinguish between
53 mega-dunes and other forms of periodic, or “transversal” dunes that mainly form in the coastal zone of
54 East Antarctic Ice Sheet and differ from mega-dunes in their morphology and, likely, origin.

55 The first observations of relationship between the ice sheet surface topography (surface slope) and
56 snow accumulation rate have shown that in all types of the dunes the snow is subjected to a very strong
57 aeolian redistribution with the increased accumulation in the concaves and reduced accumulation on
58 the convexities (Black and Budd, 1964). This relationship has been later confirmed in a number of
59 studies, e.g. (Frezzotti et al., 2007;Fujita et al., 2011;Hamilton, 2004;Kaspari et al., 2004;Richardson et
60 al., 1997;Rotschky et al., 2004;Anschutz et al., 2007;Ekaykin et al., 2002;Dadic et al., 2013). These
61 studies have also shown that the dunes are not stagnant, but rather drift across the ice sheet surface,
62 which does not allow the snow to simply fill in the hollows between the dunes thus maintaining their
63 dynamical equilibrium. The estimates of the dunes' horizontal drift velocity ranges from 4 to 25 m yr⁻¹
64 (Whillans, 1975;Frezzotti et al., 2002b;Van der Veen et al., 1999;Black and Budd, 1964).

65 The first dedicated ground survey of mega-dunes was made by (Frezzotti et al., 2002b). It was shown, in
66 particular, that snow is removed from the leeward slopes of the dunes where specific erosional type of
67 snow, “glaze surface”, is formed. In contrast, snow accumulation is increased on the windward slopes
68 that are characterized by the depositional types of the snow microrelief.

69 Since the 1980s the mega-dunes are observed with the use of the satellite methods (Swithinbank,
70 1988;Fahnestock et al., 2000;Alberti and Biscaro, 2010;Scambos et al., 2012), which has revealed that
71 these snow features are widely presented in Antarctica occupying in total about 500,000 km².

72 The precipitated snow is not simply re-distributed in the mega-dune area. Indeed, it is widely recognized
73 that the wind-driven sublimation is an important part of the surface snow mass-balance (Bintanja and
74 Reijmer, 2001;Lenaerts et al., 2010;Thiery et al., 2012) removing from 20 to 75% of precipitation
75 (Frezzotti et al., 2007;Frezzotti et al., 2004). In the mega-dunes this figure may increase to 85 %
76 (Frezzotti et al., 2004). Thus, the wide extent of the mega-dune fields and glaze surfaces (that occupy in
77 total more than 10% of the continent area), where snow drift processes are intensified, must be taken
78 into account for correct estimate of the Antarctic surface mass balance (Scambos et al., 2012;Das et al.,
79 2013).

80 Physical properties of snow in the mega-dune areas have been studied by (Albert et al., 2004; Courville
81 et al., 2007; Severinghaus et al., 2010; Gregory et al., 2014). In particular, the snow erosion zones of
82 mega-dunes are represented by coarse-grained snow (depth hoar) characterized by increased air
83 permeability. The processes taking place in snow under near-zero accumulation help to understand the
84 data on isotopic composition of gas trapped in the ice core air bubbles (Severinghaus et al., 2010). It is
85 suggested that low-accumulation highly permeable snow zones, similar to that currently existing in the
86 mega-dune areas, had large extent in Antarctica in the glacial times (Dreyfus et al., 2010).

87 Chemical properties of the mega-dune snow were considered in very few studies (Dixon et al., 2013). It
88 is noted that the surface slope may, at least in the coastal areas, affect the snow chemistry
89 (Mahalinganathan et al., 2012).

90 The strong post-depositional metamorphosis of snow in the mega-dunes has to modify its stable water
91 isotope properties (Courville et al., 2007; Frezzotti et al., 2002b; Neumann et al., 2005). It is also known
92 that irregular snow redistribution by wind due to complex surface topography does affect the isotopic
93 content of the deposited snow, which cause a poor correlation of isotopic profiles obtained in two
94 points separated by only a short distance (Ekaykin et al., 2014; Benoist et al., 1982; Karlof et al., 2006).
95 However, no systematic study of snow isotopic composition in the mega-dunes has been conducted up
96 to now.

97 In the summer seasons of 58th, 59th and 60th Russian Antarctic Expeditions (RAE), 2013-2015, we carried
98 out complex glaciological investigations in the mega-dune area located about 30 km to the East from
99 Russian Vostok Station (Fig. 1). In this paper we analyze the spatial distribution of the snow isotope
100 content in the mega-dunes.

101

102 **2 Data and methods**

103 **2.1 Glaciological and stable water isotope data**

104 In January 2013 the Vostok mega-dune area was visited for the first time. The accumulation-stake
105 profile was established perpendicular to the mega-dune crest. The total number of stakes was 21
106 (named MD00 to MD20), the distance between adjacent stakes was about 100 m, and the total length of
107 the profile was 1983 m (Fig. 1). The samples of the upper 1.5 m of snow were also taken near each stake
108 to be analyzed for the concentration of the stable water isotopes (δD , $\delta^{18}O$ and $\delta^{17}O$).

109 In January 2014 and January 2015 the stakes were revisited, and the repeated measurements of their
110 heights and surface snow density allowed to obtain the amount of snow accumulated during 2 years
111 (January 2013 - January 2015). The snow samples were taken again for chemical and isotopic analyses.

112 In January 2015 we also drilled a 20-m borehole in point MD00 (Fig. 1). In the obtained firn core we
113 measured snow density and took samples for stable water isotope analysis with a resolution of 10 cm.

114 The concentration of heavy water isotopes (δD and $\delta^{18}O$) in 42 snow surface samples taken in 58th and
115 59th RAE, as well as in 183 samples from MD00 core, was measured at Climate and Environmental
116 Research Laboratory (CERL) using a Picarro L2120-*i* analyzer. Our working standard (VOS), measured
117 after every 5 samples, was made of the light Vostok snow and calibrated against the IAEA standards
118 VSMOW-2, GISP and SLAP-2. The reproducibility of results defined by re-measurements of randomly
119 chosen samples was 0.04 ‰ for $\delta^{18}O$ and 0.2 ‰ for δD , which is 2 orders of magnitude less than the

120 natural variability of the snow isotopic composition (see below) and thus satisfactory for the purposes of
121 the study.

122 In October 2015 we also measured ^{17}O -excess values in the samples collected during the 59th RAE using
123 a Picarro L2140-*i* analyzer. For this, each sample was measured 15 times in the high-precision mode and
124 we took an average of the last 10 measurements. Every 3 samples we measured the VOS standard
125 previously calibrated against VSMOW-2, GISP and SLAP-2 (taking into account that they have ^{17}O -excess
126 values of, correspondingly, 0, 22 and 0 per meg (Schoenemann et al., 2013)). The ^{17}O -excess value of
127 VOS was found to be 0 per meg, similar to SLAP. The reproducibility of the ^{17}O -excess values of
128 individual samples was 8 per meg.

129 All the data discussed in this paper is presented in Table 1.

130

131 **2.2 GNSS positioning**

132 The absolute altitude and location was determined with high accuracy along the profile using the
133 geodetic GPS technique.

134 Therefore the Bernese GPS Software 5.1 (Dach et al., 2007) was used to process the two kinematic GNSS
135 profiles (K58B and K58C) as a combined differential solution from GPS and GLONASS observations. As
136 reference stations for this network solution we used two local receivers at Vostok station in a distance
137 of 30km and additional two reference stations at the coast with baseline lengths of about 1350 km (near
138 the Russian research stations Progress and a station of the global IGS-network near the Australian
139 Station Casey). After reducing the antenna positions to the snow surface we estimated the accuracy by
140 calculating the height differences at track crossovers. Crossovers inside one track imply an internal RMS
141 of the differences of 2.9 cm (at 160 crossover points) for track K58B and 2.4 cm (at 9 crossover points)
142 for track K58C. With a RMS of 7.7cm at 5159 crossovers between the two tracks we can estimate the
143 absolute precision of a single kinematic surface height according to the variance propagation to about
144 5.4 cm.

145

146 **2.3 GPR data**

147 During the austral summer field season of the 58th Russian Antarctic Expedition (January 2013) the GPR
148 profiling was performed to study the snow-firn layer structure of the mega-dune area. The 200 MHz
149 GSSI SIR10B GPR with "5106 200 MHz" antenna was applied.

150 The GPR equipment was installed on 2 sledges towed by a ski-doo. The route of the GPR profiling was
151 the same with the geodetic observations. In total, about 80 km of the GPR profiles were obtained (Fig.
152 1), though in this paper we only use the 2-km section obtained along the glaciological profile (points
153 MD00-MD20 in Fig. 1).

154 The main problem in the processing and interpretation of the GPR data is the dielectric properties of the
155 media where the electromagnetic waves propagate. We used the model published in (Popov and
156 Eberlein, 2014) to transform the radio-echo time-section (Fig. 2) into the depth section. To calculate the
157 vertical electromagnetic wave speed we used the firn density data measured in MD00 core.

158 In Fig. 2 we show the GPR registration recorded along the glaciological profile (MD00-MD20).

159

160 **3 Results**

161 The mega-dune formation is related to a sharp increase of the ice sheet slope in the prevailing wind
162 direction (SPWD) (Frezzotti et al., 2002b). The Vostok mega-dunes are not an exception, as they form
163 leeward from the eastern shore of the Lake Vostok, where the SPWD changes from near zero or even
164 negative values (interestingly, in the closest vicinities of Vostok Station the wind is blowing uphill) to
165 about 1.6 m km^{-1} . The latter figure generally agrees with the Frezzotti and others' (2002) conclusion that
166 the mega-dunes only develop where the SPWD is from 1 to 1.5 m km^{-1} .

167 The wavelength of the Vostok mega-dunes are about 1.9 km, and the amplitude (the elevation change
168 between the dune crest and the nearest windward hollow) is about 1.2 m, i.e., they are relatively small
169 compared to those reported in the above mentioned studies.

170 Below we present the results of the glaciological investigations in the Vostok mega-dune area (Fig. 3).

171

172 **3.1 Accumulation rate and isotopic content of snow in mega-dunes**

173 Due to the subsequent measurements of the heights of the stakes established across the mega-dunes,
174 we were able to define the snow accumulation between January 2013 and January 2015 (Fig. 3e). One
175 may clearly see the regular spatial variability of the snow build-up. In accordance with the previous
176 studies (see the review in Introduction), the snow is removed from locations with the increased surface
177 slope (leeward side of the dunes) and deposited where the slope is decreased or inverted (hollow
178 between dunes and windward side of the dunes). In a distance of few hundred meters the accumulation
179 changes by an order of magnitude, from -0.5 to 16 cm of snow (or from -0.2 to 58 mm w.e. according to
180 the surface snow density, Fig. 3d). This range is larger than that reported by (Frezzotti et al., 2002b)
181 (from 7 to 35 mm). The mean annual accumulation over one dune wavelength is 22 mm, which is very
182 similar to the accumulation at the Vostok stake network (23 mm). If the precipitation rate at Vostok
183 station and in the mega-dune area was the same, then our result does not support the observation that
184 over the mega-dune areas the accumulation is reduced due to the wind-driven sublimation (Frezzotti et
185 al., 2004).

186 Snow accumulation variability observed at the stakes during only 2 years of observations may not
187 adequately represent the long-term average due to very large random component. We used the GPR
188 data (Fig. 3g) and data on firn density from the 20-m core in order to evaluate spatial variability of the
189 multi-year average of the snow accumulation rate. The first internal reflection horizon (estimated age is
190 about 130 years, see below) is located at the depth that varies from 3 to 11 m. Thus, mean 130-year
191 snow accumulation rate varies between 1 and 35 mm w.e. over one full dune wavelength, with an
192 average of 21 mm w.e. Thus, the multi-year spatial variability of snow accumulation rate is considerably
193 smaller than that obtained from 2-year stake measurements, but still larger than that reported by
194 (Frezzotti et al., 2002b).

195 The surface snow density does not show any distinct spatial variability (Fig. 3d). The mean snow density
196 (0.355 g cm^{-3}) is slightly higher than that measured at Vostok stake network (0.33 g cm^{-3}).

197 During the field work seasons we also did not observe big difference between snow surface character in
198 leeward and windward slopes of the dunes (Fig. 4). The erosion zone does not demonstrate the

199 dominance of the glaze surface, and no big sastrugi are observed in the accumulation zone, as reported
200 by (Frezzotti et al., 2002b) for the Victoria Land mega-dune field. The small difference in snow
201 morphology between low- and high-accumulation zones of the dune may be related to the relatively
202 small dune size, although it does not explain rather big spatial variability of snow accumulation.

203 The spatial variability of the accumulation rate covaries well with the surface slope: the smaller is the
204 slope, the higher is accumulation (Fig. 3 f and e).

205 In Fig. 3a-c we show the isotopic composition (δD , d_{xs} and ^{17}O -excess) of the upper 1.5 m of snow
206 sampled twice near each point of our profile. One can see a wave in snow isotopic content (δD) with the
207 magnitude of about 25 ‰ and the wavelength similar to that of the mega-dune. The spatial variability of
208 the snow isotopic composition in the mega-dune area is significantly larger than in the area outside the
209 mega-dunes. For example, the standard deviation of the δD values in the samples representing upper
210 1.5 m of snow and taken along a 40-km profile in the southern part of Lake Vostok, where the glacier is
211 characterized by flat surface, is ± 4 ‰ (Ekaykin et al., 2012) against ± 6 ‰ in the mega-dune area.
212 Another difference is that outside the mega-dunes the variability of snow isotopic composition is
213 random, with no clear periodicity. At the same time, the average values of δD are similar in both cases,
214 around -440 ‰.

215 There is a negative covariation between snow isotopic composition and accumulation rate (correlation
216 coefficient, -0.38, is not statistically significant due to the small number of points).

217 We explain this behavior of the snow isotopic composition by different post-depositional alteration of
218 the initial isotopic composition of snow precipitation deposited in the low- and high-accumulation zones
219 of the mega-dunes. Indeed, the erosion zone is characterized by "a long, multiannual, steep
220 temperature-gradient metamorphism" (Frezzotti et al., 2002b), page 8. Thus, the snow here should be
221 enriched in heavy isotopes due to strong post-depositional modification (Town et al., 2008) that may be
222 further facilitated by the increased permeability of the snow in such locations (Albert et al., 2004). We
223 may speculate that in the mega-dunes described by (Frezzotti et al., 2002b), characterized by a very
224 strong modification of the snow physical properties, the isotopic transformation should be even
225 stronger than in the Vostok dunes.

226 An alternative explanation of negative spatial relationship of isotopic composition and snow
227 accumulation was suggested by (Ekaykin et al., 2002). Since in winter the snow crystals are smaller and
228 wind speed is higher, this snow could be easier re-distributed by wind comparing to snow precipitated in
229 summer. If so, in the erosion zone of the mega-dunes the proportion of summer snow is larger than in
230 the accumulation zone.

231 We may use the isotopic data to determine which mechanism, "post-depositional" or "re-distributional"
232 (or both) is mainly responsible for the anomaly of the snow isotopic composition in the mega-dune area.

233 The observed $d_{xs}/\delta D$ and ^{17}O -excess/ δD slopes (ratios between the standard deviations of the
234 smoothed profiles shown in Fig. 3a, b and c) are, correspondingly, -0.2 ‰/‰ and 0.9 per meg/‰.
235 During the post-depositional changes of the snow isotopic composition these slopes are -0.2 ‰/‰ and
236 0.4 per meg/‰ (Ekaykin et al., 2016). During the seasonal cycle of the isotopic composition of snow
237 precipitation at Vostok, these parameters are related by slopes -0.1 ‰/‰ and 0.4 per meg/‰ (Landais
238 et al., 2012).

239 Thus we may conclude that the mixing of the summer and winter precipitation in different proportions
240 cannot explain the variability of snow isotopic composition observed in the mega-dune area, since the
241 variability of ^{17}O -excess and of δx_s in this case would be significantly smaller. The post-depositional
242 factor would better explain the observed snow isotopic composition in the mega-dunes, but still the
243 variability of ^{17}O -excess seems to be too strong. Note, however, that the data by (Ekaykin et al., 2016)
244 were obtained in laboratory experiments, not in natural conditions, so the ^{17}O -excess/ δD slopes
245 reported there may be underestimated.

246 We should also note that the ^{17}O -excess values positively covariate with the accumulation rate (Fig. 3 c
247 and e), though one would expect a negative covariation in case if the snow isotopic composition
248 variability is due to the post-depositional processes. At present we do not know if this positive
249 covariation is caused by errors in the ^{17}O -excess values, or it suggests another mechanism that creates
250 isotopic anomalies in the mega-dune area.

251

252 **3.2 Mega-dune drift**

253 We used the GPR data to reconstruct the previous positions of the dunes, and to calculate the velocity
254 of the dunes drift.

255 In the GPR profile taken across the mega-dunes (Fig. 2), we see several distinct internal reflection
256 horizons (IRH). For 7 of them we defined the depths (Table 1) and, subtracting these depths from the ice
257 sheet elevation, we could define the absolute altitude of each IRH (Fig. 3g). Thus we can see the buried
258 surfaces of our dune and may trace its drift in time.

259 For this, we first need to date each IRH. We used the density profile obtained from the MD00 core and
260 the average snow accumulation rate in the mega-dune area in order to calculate the depth-age function
261 and determine the age of each IRH (Fig. 3g). The uppermost IRH marks the surface of the dune about
262 130 years ago, and the lowermost – 530 years ago.

263 We chose 3 fold hinges (the summit of crests and two lowest points of the fold dips) to trace the dune
264 drift. On average, the dune is drifting upwind with the rate of $4.6 \pm 1.1 \text{ m yr}^{-1}$. This corresponds very well
265 with the value reported by (Frezzotti et al., 2002b), 5 m yr^{-1} . With this velocity a dune drifts by one full
266 wavelength in about 410 years.

267 As pointed by (Arcone et al., 2005), the apparent dune drift velocity observed in the GPR images is a
268 combination of the real dune velocity and the ice movement, and the real dune velocity is higher than
269 the observed one. According to (Richter et al., 2013), ice flow velocities in this region do not exceed 2 m
270 yr^{-1} , so the real dune drift velocity could be up to 6.6 m yr^{-1} . However, the ice is moving almost in parallel
271 with the dune crests (from north-west to south-east). So, the projection of the ice speed vector on the
272 MD profile is close to 0 m yr^{-1} , and the correction to the dune drift velocity due to the ice movement
273 should be close to zero, too. Finally, for the purposes of our study we need not real, but the resultant
274 dune velocity observed by GPR, so in the further calculations we use the apparent dune velocity of 4.6
275 m yr^{-1} .

276

277 **3.3 Non-climatic temporal oscillation related to the mega-dune drift**

278 When the dune drifts, the spatial anomalies in snow physical properties, accumulation rate and isotopic
279 composition are drifting accordingly. For example, the point MD00, now located at the leeward side of
280 the dune with reduced accumulation and enriched isotopic composition, about 300 years ago was in the
281 hollow between dunes with increased accumulation and lower heavy isotope content. If one drills an ice
282 core in the mega-dune area, he would see a quasi-periodic (with the period of 410 years) oscillations in
283 snow accumulation and isotopic composition related to the dune drift.

284 Let us simulate such an oscillation that we would see in a core drilled at MD00 point.

285 In Fig. 5a we showed a temporal variability of snow accumulation (blue) and isotopic composition (red)
286 that should be seen in point MD00 when the dune crosses this point. To construct these curves, we
287 simply divided the distance of each point in Fig. 3 a and e by the above mentioned velocity of the dune
288 drift. We also showed in Fig. 5a the climatic variability in Vostok region over the same time interval
289 (Ekaykin et al., 2014) in purple. Note that the amplitudes of the both components are similar.

290 Combining the dune-related and climatic components, we obtain the expected temporal variability of
291 snow isotopic composition in MD00 (Fig. 5b). Then we transform it to a vertical isotopic profile using the
292 depth-age function presented in Fig. 5c. This function takes into account the significant dune-related
293 variability in snow accumulation rate (Fig. 5a), this is why it is essentially non-linear. The resulting
294 simulated vertical isotopic profile is presented in Fig. 5d by red line. In the upper part of the profile the
295 isotopic oscillations are compressed due to the low accumulation rate, and deeper, when the
296 accumulation is higher, they are stretched.

297 In our simulations we do not take into account that the mega-dune snow may experience enhanced
298 diffusive smoothing due to the increased ventilation of the snow column. In this case the isotopic profile
299 could be substantially smoothed.

300 In Figure 5d we also showed by the blue line the real isotopic profile from the MD00 core. One can see a
301 good resemblance between them, except for the very bottom part of the MD00 core. Indeed, at the
302 depth of 20 m the core has a δD isotopic composition of -420 ‰. Neither climatic record, nor the
303 isotopic profile from the mega-dunes (Fig. 5a) demonstrate such high isotopic value, this is why we
304 could not reproduce it in our simulations.

305

306 **4 Discussion - Non-climatic variability in ice cores**

307 In the previous sections we demonstrated that the snow isotopic composition has significant spatial
308 variability in the mega-dune area, suggested a possible mechanism to explain this variability, and then
309 explained how this "dune-related" signal is transferred to a firn core isotopic profile. We calculated an
310 artificial firn core isotopic profile in the mega-dune area and compared it with the real firn core isotopic
311 profile.

312 In the case of MD00 core we know that the "signal" we see is mostly related to a dune drift, but how can
313 one separate the climatic signal from non-climatic variability in real ice cores?

314 Indeed, it is commonly understood that a mega-dune area is an unsuitable place to drill ice for climatic
315 studies, but it does not mean that the locations outside the mega-dune fields are free from non-climatic,
316 "relief-related" variability.

317 As an example we may mention the South Pole Station region that is not a mega-dune area, but detailed
318 topographic survey shows mega-dune-like features with a typical amplitude of few meters and
319 wavelength of several kilometers – see Fig. 8 in (Van der Veen et al., 1999) and Fig. 2 in (Hamilton,
320 2004). Unlike the mega-dunes, these snow hills are not elongated, but rather round in shape. The
321 authors suggest these structures are not stationary, but slowly change their locations, which causes
322 temporal non-climatic variability of snow accumulation rate with the period of several hundred or few
323 thousand years. Very similar structures are observed around the Kohnen Station (Eisen et al., 2005) and
324 in West Antarctica (Arcone et al., 2005).

325 Even the vicinities of the main domes cannot be considered as “dune-safe”. Indeed, the study of the
326 snow isotopic composition profile in two neighboring cores drilled about 55 km to the north-east from
327 the summit of Dome C showed a very low signal-to-noise ratio likely related to the local ice sheet
328 topography (Benoist et al., 1982).

329 In Dronning Maud Land the ice cores drilled in relatively short distance one from another demonstrate
330 opposite trends in the snow accumulation rates over the past 200 years (Oerter et al., 2000), which may
331 be considered as the influence of the non-climatic factors.

332 In general, in low-accumulation sites signal-to-noise ratio in both snow accumulation rate and isotopic
333 composition is very small, being of the order of 0.2 (Ekaykin et al., 2014). The noise, related to the snow
334 re-distribution by wind and/or post-depositional processes, is larger than the climatic signal even at the
335 centennial scale. This means that to study climatic variability with the periods less than $10^3 - 10^4$ years in
336 the low accumulation area (which comprises most of the East Antarctica (Arthern et al., 2006)) more
337 than one ice core should be investigated for each location.

338 The influence of snow topography on snow accumulation is known and to large extent understood on
339 the spatial scale from 10^2 to 10^1 m (micro-relief) and from 10^3 to 10^6 m (mega-dunes and continental
340 scale). However, very little is known about the scale from 10^1 to 10^3 m, the range of “meso-dunes”
341 (Ekaykin et al., 2002; Eisen et al., 2008). Meso-dunes are relatively small forms (with typical wavelengths
342 from 200 to 300 m) of snow relief observed in the vicinities of Vostok Station. It was shown that the
343 meso-dunes cause a spatial variability of snow properties: on the bumps the snow accumulation is
344 lower, and its isotopic composition is higher, while in the hollows between the dunes more snow
345 accumulates with lower concentration of heavy isotopologues (Ekaykin et al., 2002). Since these dunes
346 seem to be not stagnant, it is likely that the drift of the meso-dunes causes the non-climatic temporal
347 oscillations of snow isotopic composition and accumulation rate with a period of few decades due to
348 mechanisms similar to those described in this paper for the mega-dunes. Further studies of this
349 phenomenon are needed.

350

351 **Conclusion**

352 The ice cores are priceless source of numerous and diverse paleo-climatic data, and this will hold true
353 even despite the unavoidable limitations. One of the most important limitations is related to a high level
354 of noise which contaminates the climatic signal on relatively short time scales (years to millennia),
355 especially in the low-accumulation areas. The main reason of this noise is a complex snow/ice sheet
356 topography that leads to snow re-distribution due to wind activity, which is further complicated by the
357 post-depositional processes.

358 In this paper we present the results of the field works carried out during three Antarctic summer
359 seasons in the vicinity of Vostok Station. We mainly deal with the influence of large snow relief forms,
360 mega-dunes, on the snow isotopic composition. We demonstrate that the leeward sides of the dunes
361 are characterized by reduced accumulation and increased concentration of heavy water molecules likely
362 due to post-depositional alteration of the snow isotopic content. In opposite, windward sides of the
363 dunes accumulate more snow that is enriched in light water isotopes.

364 Using the GPR data, we were able to trace the drift of the dunes and to calculate their velocity, 4.6 ± 1.1
365 m yr^{-1} . This allowed us to simulate the temporal variability of the snow isotopic composition that would
366 be observed in a given point due to the passing of the mega-dune across this point. Then we compared
367 this artificial vertical profile of the snow isotopic composition with the real isotopic data from a firn core
368 drilled in the mega-dune cite. We showed that the two profiles are very similar.

369 As a result of our study we come to the following conclusions:

370 1) For the first time we demonstrated that snow isotopic composition has significant spatial variability in
371 the mega-dune area in covariance with the snow accumulation rate and surface slope, although the
372 mechanism that forms this variability is yet to be clarified. We also demonstrated how these spatial
373 waves are transformed into the oscillations of snow isotopic composition in a firn/ice core vertical
374 profile.

375 2) Based on published data we may conclude that significant (periodic or non-periodic) spatial variability
376 is widespread in Antarctica, even outside the mega-dune areas. The drift of different types of dunes
377 across the snow/ice sheet surface causes non-climatic temporal variability of snow accumulation rate
378 and isotopic composition, as observed in firn or ice cores, thus considerably reducing the signal-to-noise
379 ratio on the timescales from decades to millennia.

380 3) The only robust way to obtain a reliable climatic signal is to investigate several ice cores and to
381 construct a stack record of studied parameters.

382 We also suggest that the mega-dunes are a unique environment that provides the necessary conditions
383 to test different hypothesis. For example, in a short distance one can find locations absolutely different
384 in terms of snow accumulation rate, isotopic composition, physical and (likely) chemical properties,
385 which could be used to study the post-depositional processes, to model glacial conditions (Severinghaus
386 et al., 2010) etc.

387 In the future studies we plan to investigate the spatial variability of chemical content, the concentration
388 of microparticles and other compounds in the surface snow in the Vostok mega-dune area.

389

390 **Acknowledgement**

391 We thank O. Eisen, M. Frezzotti, T. Scambos and M. Schneebeli for numerous corrections and
392 suggestions that allowed to improve significantly the manuscript.

393 The logistic operations in Antarctica were provided by Russian Antarctic Expedition. We personally thank
394 Vitaly Zarovchatskiy for his help in the field works. The authors are grateful to Anna Kozachek and Diana
395 Vladimirova (CERL) for the high-quality isotopic data. We also thank Achille Zirizzotti and Stefano Urbini
396 (Istituto Nazionale di Geofisica e Vulcanologia, Rome, Italy) for providing the GPR equipment.

397 This study was completed at the expense of the grant of Russian Science Foundation (project 14-27-
398 00030).

399

400 **Figure captions**

401

402 Figure 1. Vicinities of Vostok Station and the location of the study area.

403 The mega-dunes are highlighted by hatching. Black line is the route of GPR and geodetic profiles. The
404 location of the glaciological profile is shown in the insert (MD00-MD20). White line is the Vostok lake
405 shoreline adapted from (Popov and Masolov, 2007).

406

407 Figure 2. GPR registration recorded along the MD00 profile.

408

409 Figure 3. The results of the glaciological, GPR and geodetic survey in the Vostok mega-dune area.

410 a - c – isotopic content of the surface (1.5 m) layer of the snow thickness, δD (a), dxs (b) and ^{17}O -excess
411 (c). For δD the points show the individual samples and the red line is the average of the 58 and 59 RAE
412 samples. For dxs only the average is shown. Note that the dxs axis is reversed. For ^{17}O -excess we showed
413 the 5-point running means with the error bars ($\pm 1\sigma$, where σ is the error of the average of 5 individual
414 values).

415 d – surface (20 cm) snow density, individual values (points) and 3-point running mean (line).

416 e – mean snow build-up in 2013-2014, individual values (points) and 3-point running mean. Dashed lines
417 show the confidence interval ($\pm 1 \sigma$) of 2-year average accumulation value as deduced from Vostok stake
418 network. Note that the Y axis is reversed.

419 f – surface slope calculated over 20-m intervals of the ice sheet surface. Negative values mean that the
420 local slope is the opposite of the general slope in this region (from south-west to north-east).

421 g – the elevation of the ice sheet surface and of 7 internal reflection horizons (IRH) above sea level
422 defined by the geodetic measurements and GPR survey.

423 The gray shading depicts the snow layer (1.5 m) in which the snow isotopic content was measured. The
424 dashed lines connect the fold hinges used to calculate the dune drift velocity. The values to the right are
425 the estimated ages of each IRH relative to January 2015.

426 The profile is spread from south-west (left part of the figure) to the north-east (right part), see Figure 1.
427 The individual values shown in Figure 3 can be found in Table 1.

428

429 Figure 4. Photo of the snow surface in points MD02 (a) – erosion zone, leeward slope of the dune – and
430 MD13 (b) – deposition zone, the hollow between dunes.

431

432 Figure 5. Simulated isotope profile in MD00 point.

433 a – the values of snow accumulation rate (blue) and isotopic composition (red) that could be observed in
434 point MD00 if one would measure them as long as the dune travel across this point. To calculate this we
435 used the data from Fig. 3 a and e, and data on the dune drift velocity. Purple – climatic variability of the
436 snow isotopic composition in the Vostok region taken from (Ekaykin et al., 2014).

437 b – a combination of climatic and dune-related isotopic variability (red + purple from Fig. 5a).

438 c – depth-age function for the snow thickness in point MD00.

439 d – simulated vertical profile of snow isotopic composition calculated using the data from Fig. 5b and
440 depth-age function (Fig. 5c), in red, compared with the real vertical profile of snow isotopic composition
441 measured in the core drilled in point MD00, in blue.

442

- 445 Albert, M., Shuman, C., Courville, Z., Bauer, R., Fahnestock, M., and Scambos, T.: Extreme firn
446 metamorphism: Impact of decades of vapor transport on near-surface firn at a low-accumulation glazed
447 site on the East Antarctic plateau, *Ann. Glaciol.*, 39, 73-78, 2004.
- 448 Alberti, M., and Biscaro, D.: Height variation detection in polar regions from icesat satellite altimetry,
449 *Computers and Geosciences*, 36, 1-9, 2010.
- 450 Anschütz, H., Eisen, O., Rack, W., and Scheinert, M.: Periodic surface features in coastal East Antarctica,
451 *Geophys. Res. Lett.*, 33, 1-5, 2006.
- 452 Anschütz, H., Eisen, O., Oerter, H., Steinhage, D., and Scheinert, M.: Investigating small-scale variations
453 of the recent accumulation rate in coastal Dronning Maud Land, East Antarctica, *Ann. Glaciol.*, 46, 14-21,
454 2007.
- 455 Arcone, S. A., Spikes, V. B., and Hamilton, G. S.: Stratigraphic variation within polar firn caused by
456 differential accumulation and ice flow: Interpretation of a 400 MHz short-pulse radar profile from West
457 Antarctica, *J. Glaciol.*, 51, 407-422, 2005.
- 458 Arthern, R. J., Winebrenner, D. P., and Vaughan, D. G.: Antarctic snow accumulation mapped using
459 polarization of 4.3-cm wavelength microwave emission, *J. Geophys. Res.*, 111, 2006.
- 460 Benoist, J. P., Jouzel, J., Lorius, C., Merlivat, L., and Pourchet, M.: Isotope climatic record over the last 2.5
461 ka from Dome C, antarctica, ice cores, *Ann. Glaciol.*, 3, 17-22, 1982.
- 462 Bintanja, R., and Reijmer, C. H.: A simple parameterization for snowdrift sublimation over Antarctic snow
463 surfaces, *J. Geophys. Res.*, 106, 31,739-731,748., 2001.
- 464 Black, H. P., and Budd, W.: Accumulation in the region of Wilkes, Wilkes Land, Antarctica, *J. Glaciol.*, 5, 3-
465 15, 1964.
- 466 Courville, Z. R., Albert, M. R., Fahnestock, M. A., Cathles IV, L. M., and Shuman, C. A.: Impacts of an
467 accumulation hiatus on the physical properties of firn at a low-accumulation polar site, *J. Geophys. Res.*,
468 112, 1-11, 2007.
- 469 Dach, R., Hugentobler, U., Fridez, P., and Meindl, M.: Bernese GPS software version 5.0, Univ. of Bern,
470 Bern, Switzerland, 2007.
- 471 Dadic, R., Mott, R., Horgan, H. J., and Lehning, M.: Observations, theory, and modeling of the differential
472 accumulation of Antarctic megadunes, *J. Geophys. Res. Earth Surf.*, 118, 2343-2353,
473 10.1002/2013JF002844, 2013.
- 474 Das, I., Bell, R. E., Scambos, T. A., Wolovick, M., Creyts, T. T., Studinger, M., Frearson, N., Nicolas, J. P.,
475 Lenaerts, J. T. M., and Van den Broeke, M. R.: Influence of persistent wind scour on the surface mass
476 balance of Antarctica, *Nature Geoscience*, 6, 367-371, 2013.
- 477 Dixon, D. A., Mayewski, P. A., Korotkikh, E., Sneed, S. B., Handley, M. J., Introne, D. S., and Scambos, T. A.:
478 Variations in snow and firn chemistry along US ITASE traverses and the effect of surface glazing, *The
479 Cryosphere*, 7, 515-535, 2013.
- 480 Dolgushin, L. D.: Geographical observations in Antarctica. Rep. 1 (in Russian), *Izv. AN SSSR, Geography*,
481 28-47, 1958.
- 482 Dreyfus, G., Jouzel, J., Bender, M., Landais, A., Masson-Delmotte, V., and Leuenberger, M.: Firn
483 processes and $\delta^{15}\text{N}$: Potential for a gas-phase climate proxy, *Quat. Sci. Rev.*, 29, 28-42, 2010.
- 484 Eisen, O., Rack, W., Nixdorf, U., and Wilhelms, F.: Characteristics of accumulation around the EPICA
485 deep-drilling site in Dronning Maud Land, Antarctica, *Ann. Glaciol.*, 41, 41-46, 2005.
- 486 Eisen, O., Frezzotti, M., Genthon, C., Isaksson, E., Magand, O., Van den Broeke, M. R., Dixon, D. A.,
487 Ekaykin, A. A., Holmlund, P., Kameda, T., Karlöf, L., Kaspari, S., Lipenkov, V. Y., Oerter, H., Takahashi, S.,
488 and Vaughan, D. G.: Ground-based measurements of spatial and temporal variability of snow
489 accumulation in East Antarctica, *Reviews of Geophysics*, 46, 1-39, 2008.
- 490 Ekaykin, A. A., Lipenkov, V. Y., Barkov, N. I., Petit, J. R., and Masson-Delmotte, V.: Spatial and temporal
491 variability in isotope composition of recent snow in the vicinity of Vostok Station: Implications for ice-
492 core interpretation, *Ann. Glaciol.*, 35, 181-186, 2002.
- 493 Ekaykin, A. A., Lipenkov, V. Y., and Shibaev, Y. A.: Spatial distribution of the snow accumulation rate
494 along the ice flow lines between Ridge B and Lake Vostok, *Led i Sneg*, 122-128, 2012.

495 Ekaykin, A. A., Kozachek, A. V., Lipenkov, V. Y., and Shibaev, Y. A.: Multiple climate shifts in the Southern
496 Hemisphere over the past three centuries based on central Antarctic snow pits and core studies, *Ann.*
497 *Glaciol.*, 55, 259-266, 2014.

498 Ekaykin, A. A., Hondoh, T., Lipenkov, V. Y., Miyamoto, A., and Barkan, E.: Laboratory measurements of
499 the impact of sublimation on post-depositional changes in snow isotope content, 2nd IPICS Open Science
500 Conference, Hobart, 204, 2016.

501 Fahnestock, M. A., Scambos, T. A., Shuman, C. A., Arthern, R. J., Winebrenner, D. P., and Kwok, R.: Snow
502 megadune fields on the East Antarctic plateau: Extreme atmosphere-ice interaction, *Geophys. Res. Lett.*,
503 27, 3719-3722, 2000.

504 Frezzotti, M., Gandolfi, S., La Marca, F., and Urbini, S.: Snow dunes and glazed surfaces in Antarctica:
505 New field and remote-sensing data, *Ann. Glaciol.*, 81-87, 2002a.

506 Frezzotti, M., Gandolfi, S., and Urbini, S.: Snow megadunes in Antarctica: Sedimentary structure and
507 genesis, *J. Geophys. Res.*, 107, ACL 1-12, 2002b.

508 Frezzotti, M., Pourchet, M., Flora, O., Gandolfi, S., Gay, M., Urbini, S., Vincent, C., Becagli, S., Gragnani,
509 R., Proposito, M., Severi, M., Traversi, R., Udisti, R., and Fily, M.: New estimations of precipitation and
510 surface sublimation in East Antarctica from snow accumulation measurements, *Clim. Dyn.*, 23, 803-813,
511 2004.

512 Frezzotti, M., Urbini, S., Proposito, M., Scarchilli, C., and Gandolfi, S.: Spatial and temporal variability of
513 surface mass balance near Talos Dome, East Antarctica, *J. Geophys. Res.*, 112, 1-15, 2007.

514 Fujita, S., Maeno, H., Furukawa, T., and Matsuoka, K.: Scattering of VHF radio waves from within the top
515 700 m of the Antarctic ice sheet and its relation to the depositional environment: A case-study along the
516 Syowa-Mizuho-Dome Fuji traverse, *Ann. Glaciol.*, 157--164, 2002.

517 Fujita, S., Holmlund, P., Andersson, I., Brown, I., Enomoto, H., Fujii, Y., Fujita, K., Fukui, K., Furukawa, T.,
518 Hansson, M., Hara, K., Hoshina, Y., Igarashi, M., Iizuka, Y., Imura, S., Ingvander, S., Karlin, T., Motoyama,
519 H., Nakazawa, F., Oerter, H., Sjoberg, L. E., Sugiyama, S., Surdyk, S., Strom, J., Uemura, R., and Wilhelms,
520 F.: Spatial and temporal variability of snow accumulation rate on the East Antarctic ice divide between
521 Dome Fuji and EPICA DML, *The Cryosphere*, 5, 1057-1081, 2011.

522 Goodwin, I. D.: Snow accumulation and surface topography in the katabatic zone of eastern Wilkes Land,
523 Antarctica, *Antarct. Science*, 2, 235-242, 1990.

524 Gow, A. J., and Rowland, R.: On the relationship of snow accumulation to surface topography at "Byrd
525 Station", *Antarctica, J. Glaciol.*, 5, 843-847, 1965.

526 Gregory, S. A., Albert, M., and Baker, I.: Impact of physical properties and accumulation rate on pore
527 close-off in layered firn, *The Cryosphere*, 8, 91-105, 2014.

528 Hamilton, G. S.: Topographic control of regional accumulation rate variability at South Pole and
529 implications for ice-core interpretation, *Ann. Glaciol.*, 39, 214-218, 2004.

530 Karlöf, L., Winebrenner, D. P., and Percival, D. B.: How representative is a time series derived from a firn
531 core? A study at a low-accumulation site on the Antarctic plateau, *J. Geophys. Res.*, 111, 1-11, 2006.

532 Kaspari, S., Mayewski, P. A., Dixon, D. A., Spikes, V. B., Sneed, S. B., Handley, M. J., and Hamilton, G. S.:
533 Climate variability in West Antarctica derived from annual accumulation-rate records from ITASE
534 firn/ice cores, *Ann. Glaciol.*, 39, 585-594, 2004.

535 Landais, A., Ekaykin, A. A., Barkan, E., Winkler, R., and Luz, B.: Seasonal variations of ^{17}O -excess and d -
536 excess in snow precipitation at Vostok Station, East Antarctica, *J. Glaciol.*, 58, 725-733, 2012.

537 Lenaerts, J. T. M., Van den Broeke, M. R., Dery, S. J., Konig-Langlo, G., Ettema, J., and Munneke, P. K.:
538 Modeling snowdrift sublimation on an Antarctic ice sheet, 2010.

539 Mahalinganathan, K., Thamban, M., Laluraj, C. M., and Redkar, B. L.: Relation between surface
540 topography and sea-salt snow chemistry from Princess Elizabeth Land, East Antarctica, *The Cryosphere*, 6,
541 505-515, 2012.

542 Neumann, T. A., Waddington, E. D., Steig, E. J., and Grootes, P. M.: Non-climate influences on stable
543 isotopes at Taylor Mouth, Antarctica, *J. Glaciol.*, 51, 248-258, 2005.

544 Oerter, H., Wilhelms, F., Jung-Rothenhausler, F., Goktas, F., Miller, H., Graf, W., and Sommer, S.:
545 Accumulation rates in Dronning Maud Land, Antarctica, as revealed by dielectric-profiling measurements
546 of shallow firn cores, *Ann. Glaciol.*, 30, 27-34, 2000.

547 Pettre, P., Pinglot, F., Pourchet, M., and Reynaud, L.: Accumulation distribution in Terre Adelie,
548 Antarctica: Effect of meteorological parameters, *J. Glaciol.*, 32, 486-500, 1986.

549 Popov, S. V., and Masolov, V. N.: Forty-seven new subglacial lakes in the 0-110°E sector of East
550 Antarctica, *J. Glaciol.*, 53, 289-297, 2007.

551 Popov, S. V., and Eberlein, L.: Investigation of snow-firn thickness and ground in the East Antarctica by
552 means of geophysical radar, *Led i Sneg*, 4, 95-106, 2014.

553 Richardson, C., Aarholt, E., Hamran, S.-E., Holmlund, P., and Isaksson, E.: Spatial distribution of snow in
554 western Dronning Maud Land, East Antarctica, mapped by a ground-based snow radar, *J. Geophys. Res.*,
555 102, 20343-20353, 1997.

556 Richter, A., Fedorov, D. V., Fritsche, M., Popov, S. V., Lipenkov, V. Y., Ekaykin, A. A., Lukin, V. V., Matveev,
557 A. Y., Grebnev, V. P., Rosenau, R., and Dietrich, R.: Ice flow velocities over Vostok Subglacial Lake, East
558 Antarctica, determined by 10 years of GNSS observations, *J. Glaciol.*, 59, 315-326,
559 10.3189/2013JoG12J056, 2013.

560 Rotschky, G., Eisen, O., Wilhelms, F., Nixdorf, U., and Oerter, H.: Spatial distribution of surface mass
561 balance on Amundsenisen Plateau, Antarctica, derived from ice-penetrating radar studies, *Ann. Glaciol.*,
562 39, 265-270, 2004.

563 Scambos, T. A., Frezzotti, M., Haran, T. V., Bohlander, J., Lenaerts, J. T. M., Van den Broeke, M. R., Jezek,
564 K., Long, D., Urbini, S., Farness, K., Neumann, T., Albert, M., and Winther, J.-G.: Extent of low-
565 accumulation 'wind-glaze' areas on the East Antarctic plateau: Implications for continental ice mass
566 balance, *J. Glaciol.*, 58, 633-647, 2012.

567 Schoenemann, S. W., Schauer, A. J., and Steig, E. J.: Measurement of SLAP2 and GISP $\delta^{17}\text{O}$ and proposed
568 VSMOW-SLAP normalization for $\delta^{17}\text{O}$ and $^{17}\text{O}_{\text{excess}}$, *Rapid Commun. Mass Spectrom.*, 27, 582-590, 2013.

569 Severinghaus, J. P., Albert, M. R., Courville, Z. R., Fahnestock, M. A., Kawamura, K., Montzka, S. A.,
570 Muhle, J., Scambos, T. A., Shields, E., Shuman, C. A., Suwa, M., Tans, P., and Weiss, R. F.: Deep air
571 convection in the firn at a zero-accumulation site, central Antarctica, *Earth and Planetary Science Letters*,
572 293, 359-367, 2010.

573 Swithinbank, C.: Antarctica, U.S. Geol. Survey Prof. Rap., 1386-B, 1988.

574 Thiery, W., Gorodetskaya, I. V., Bintanja, R., Van Lipzig, N. P. M., Van den Broeke, M. R., Reijmer, C. H.,
575 and Kuipers Munneke, P.: Surface and snowdrift sublimation at Princess Elizabeth station, East
576 Antarctica, *The Cryosphere*, 6, 841-857, 2012.

577 Town, M. S., Warren, S. G., Walden, V. P., and Waddington, E. D.: Effect of atmospheric water vapor on
578 modification of stable isotopes in near-surface snow on ice sheets, *J. Geophys. Res.*, 113, 1-16, 2008.

579 Van der Veen, C. J., Mosley-Thompson, E., Gow, A., and Mark, B. G.: Accumulation at South Pole:
580 Comparison of two 900-year records, *J. Geophys. Res.*, 104, 31067-31076, 1999.

581 Vladimirova, D. O., and Ekaykin, A. A.: Climatic variability in Davis Sea sector (East Antarctica) over the
582 past 250 years based on the "105 km" ice core geochemical data, *Geophysical Research Abstracts*, 16,
583 285, 2014.

584 Whillans, I. M.: Effect of inversion winds on topographic detail and mass balance on inland ice sheets, *J.*
585 *Glaciol.*, 14, 85-90, 1975.

586

Table 1. Glaciological, radio-echo-sounding and geodetic data used in this study

Point name	Distance from MD00 (m)	Altitude a.s.l. (m)	Stake height (cm)		Snow build-up (cm)	Mean snow density (g cm ⁻³)	Snow accumulation (mm w.e.)	Isotope content 58 RAE				Depths of internal reflection horizons (m)						
			58 RAE	60 RAE				δD	δ ¹⁸ O	dxs	¹⁷ O-excess	1st	2nd	3rd	4th	5th	6th	7th
MD00	0	3424,25	300	292	4	0,358	14	-434,3	-56,04	14,0	-5	4	8	11	14	17	19	24
MD01	88	3424,92	151	152	-0,5	0,311	-2	-437,9	-56,37	13,1	-13	6	9	12	15	18	20	25
MD02	192	3425,75	172	163	4,5	0,330	15	-436,3	-56,30	14,1	-16	7	10	13	16	18	20	25
MD03	291	3426,37	170	170	0	0,338	0	-432,8	-55,76	13,3	-6	8	11	14	17	19	20	26
MD04	393	3427,09	195	190	2,5	0,355	8	-441,5	-56,97	14,3	-9	10	12	15	17	18	19	27
MD05	493	3427,86	175,5	165	5,25	0,367	20	-434,0	-55,97	13,8	-19	11	13	15	17	18	19	28
MD06	592	3428,35	169	167	1	0,335	3	-435,8	-56,36	15,1	-16	11	13	15	16	17	18	28
MD07	690	3428,51	171,5	154	8,75	0,345	32	-444,7	-57,49	15,2	-13	11	13	14	16	17	18	28
MD08	797	3428,73	193,5	177	8,25	0,346	28	-446,9	-57,94	16,5	-13	11	13	14	15	16	17	28
MD09	894	3428,65	187,5	170	8,75	0,345	31	-442,0	-57,29	16,3	-9	10	12	13	14	15	17	27
MD10	992	3428,61	169,5	150	9,75	0,370	34	-441,2	-57,02	15,0	0	9	12	13	14	15	17	27
MD11	1066	3428,44	179	146	16,5	0,363	57	-445,1	-57,47	14,7	-9	8	10	12	14	14	16	26
MD12	1168	3428,18	162	148	7	0,330	21	-442,7	-57,27	15,5	3	7	9	11	13	14	16	25
MD13	1289	3427,64	190,5	158	16,25	0,344	55	-436,5	-56,32	14,0	-12	5	8	11	13	14	16	24
MD14	1394	3427,53	204	188	8	0,360	28	-435,2	-56,08	13,4	2	4	8	11	13	14	17	23
MD15	1493	3427,53	196	178	9	0,337	28	-428,6	-55,17	12,8	-8		8	12	14	15	17	23

MD16	1593	3427,76	171	165	3	0,385	11	-425,0	-54,62	11,9	0		9	13	15	16	18	23
MD17	1698	3428,17	157	140	8,5	0,435	32	-432,1	-55,51	11,9	-15		10	14	16	17	19	24
MD18	1796	3428,73	188	178	5	0,348	18	-435,5	-56,04	12,8	-9	3	12	15	17	18	19	25
MD19	1901	3429,6	209	201	4	0,420	13	-440,4	-56,72	13,3	8	4	13	16	18	19	20	26
MD20	1983	3430,17	184,5	172	6,25	0,335	19	-437,8	-56,38	13,3	-10	10	15	18				29

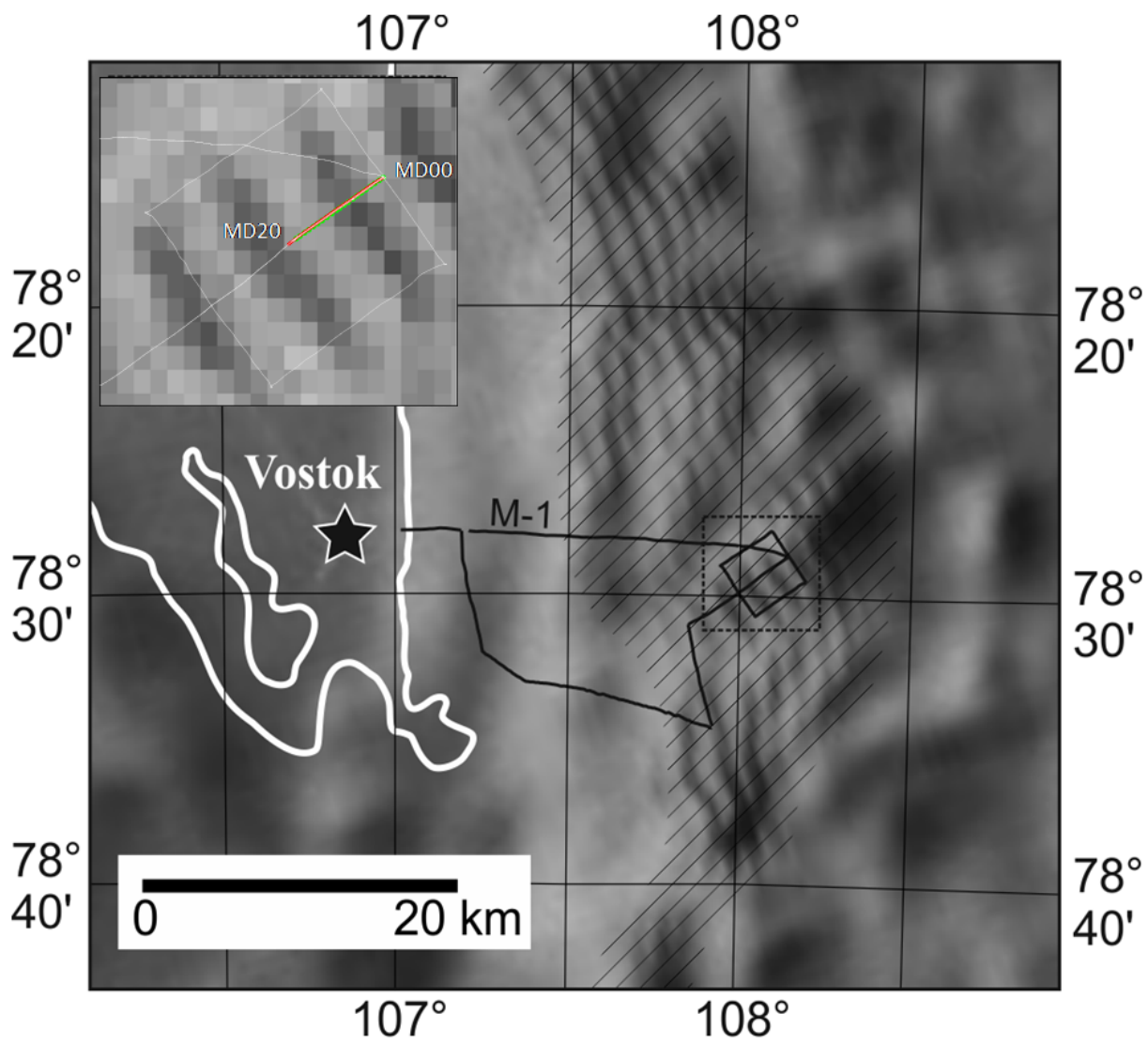


Figure 1.

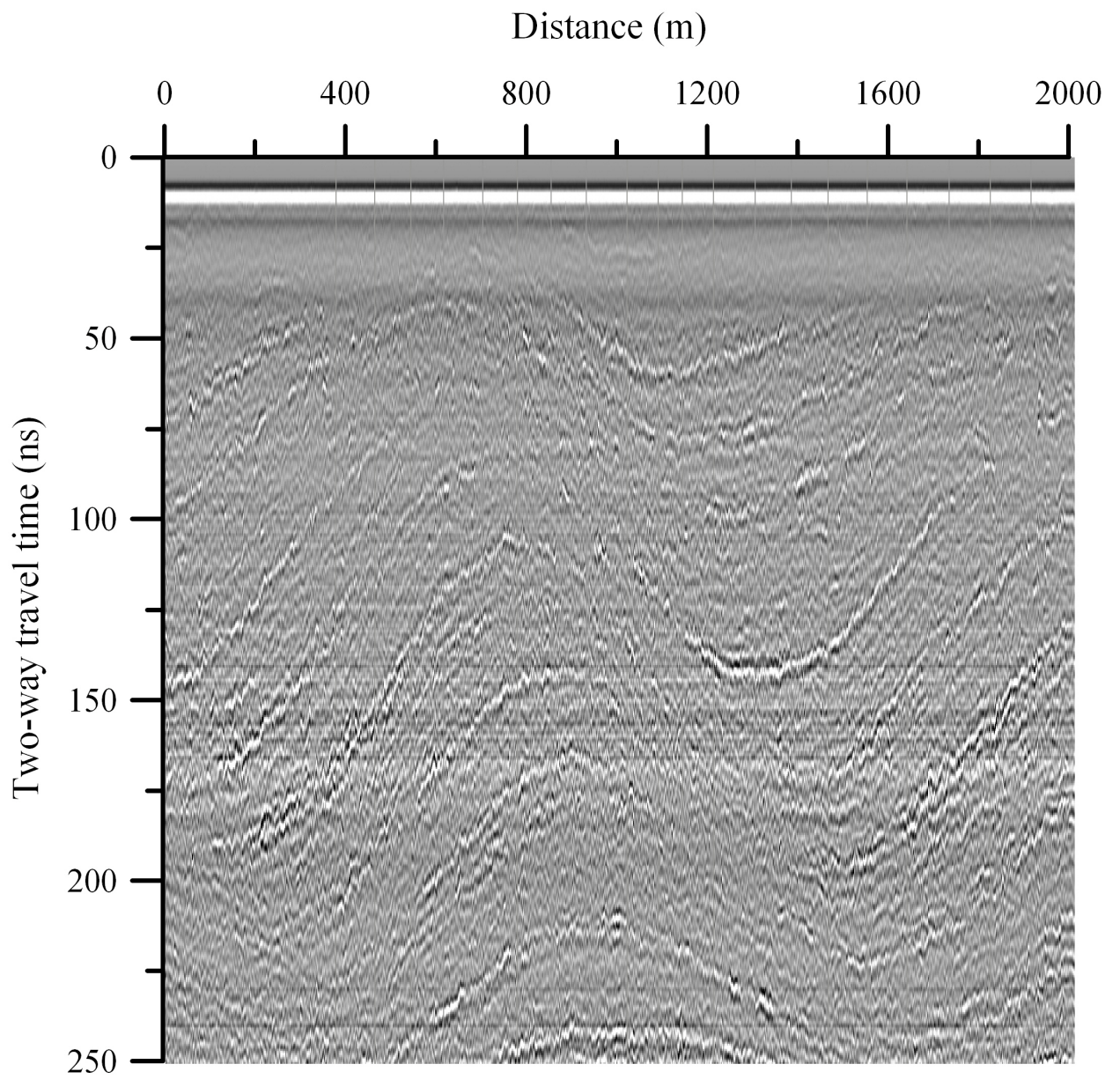


Figure 2.

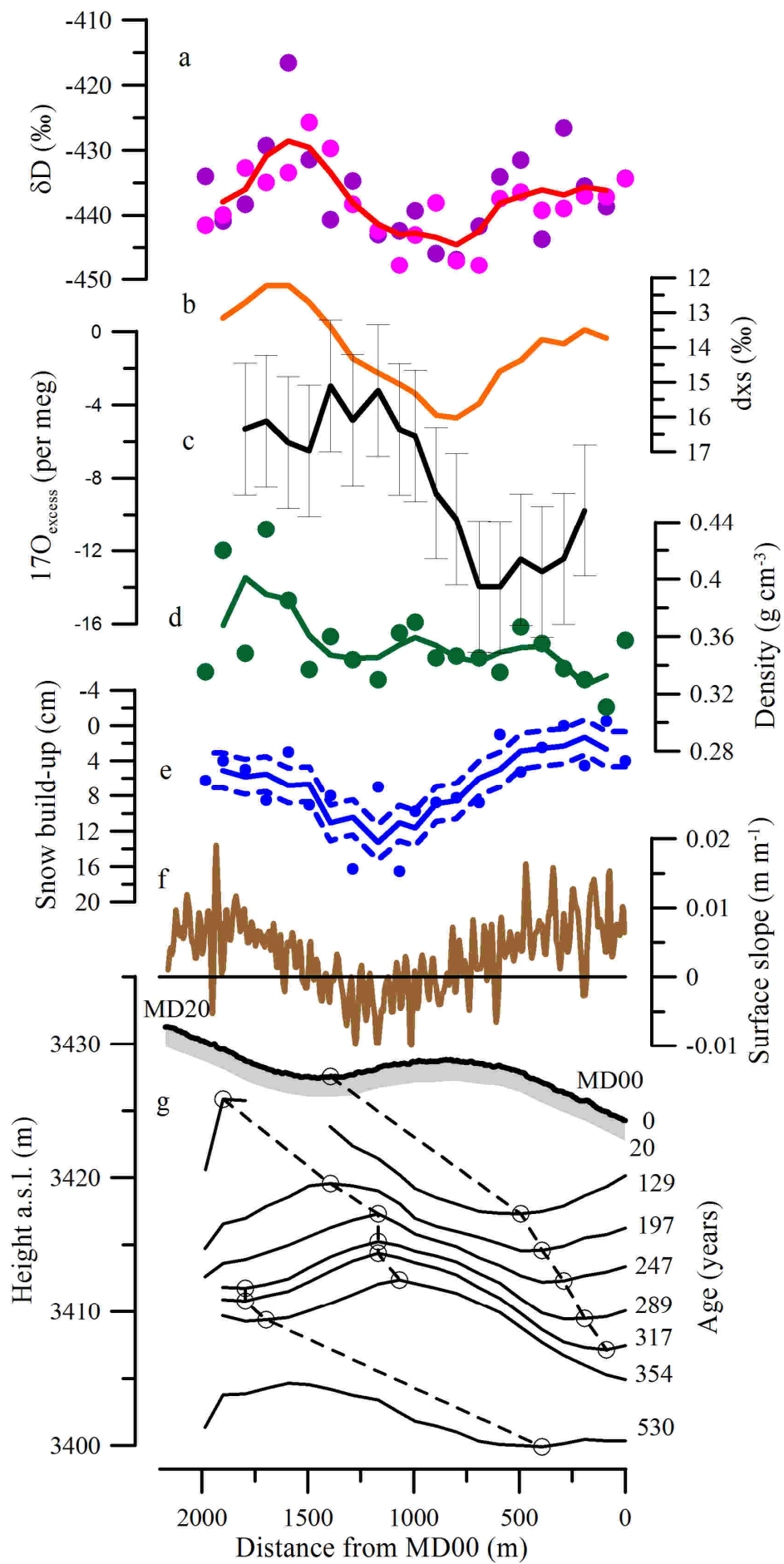


Figure 3.



Figure 4.

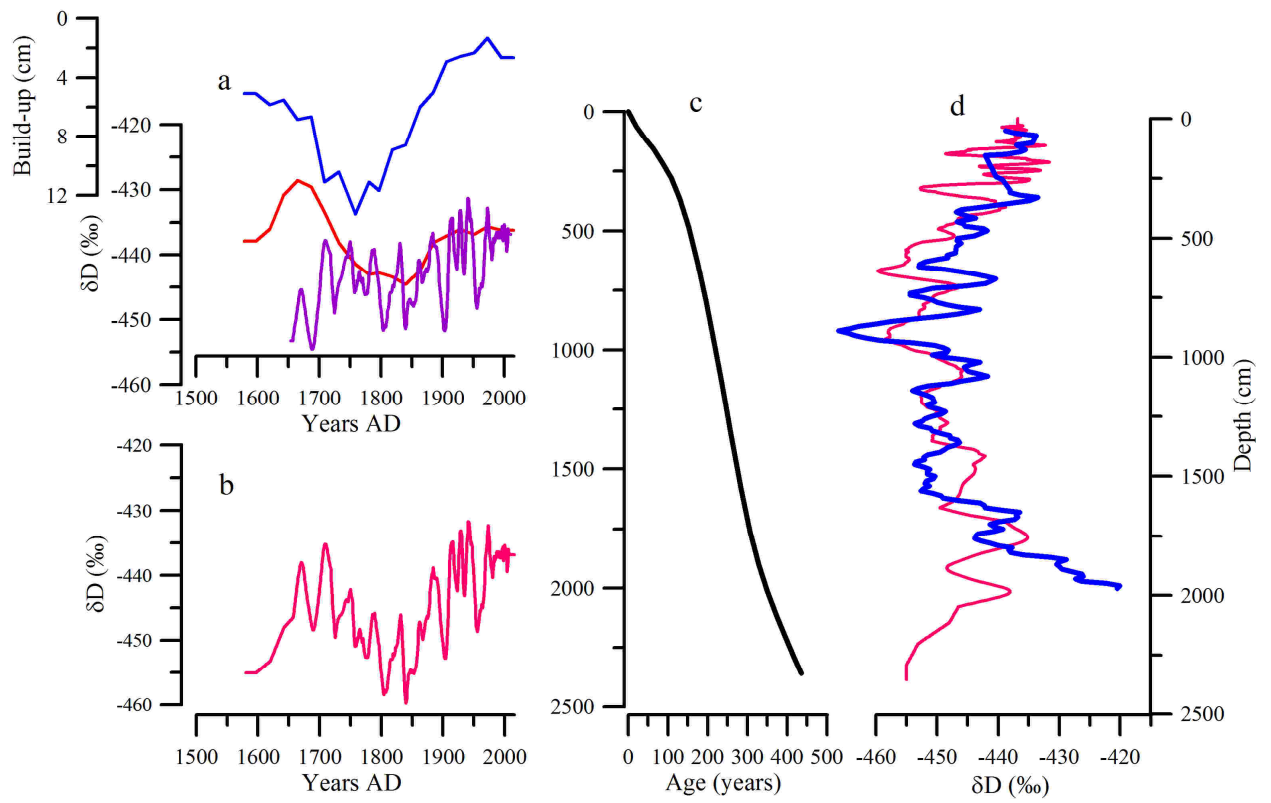


Figure 5